Analyzing the Side Force on a Baseball Using Hawk-Eye Measurements

Glenn Healey and Lequan Wang
Electrical Engineering and Computer Science
University of California, Irvine, CA 92617
Email: ghealey@uci.edu

1 Introduction

The flight of a pitch is a complicated function of the forces on the ball after it leaves a pitcher's hand. The force that the pitcher influences the most, the lift force, determines how much a pitch trajectory will change due to spin. A typical pitch is airborne for about 400 milliseconds and the batter must predict its path and start his swing within the first 200 milliseconds [3]. Small errors in prediction impair the batter's ability to make contact and, as a result, pitchers benefit from using spin to alter pitch trajectories [5].

Characteristics of the lift force, which is also known as the Magnus force, have been estimated from data acquired by the Trackman (TM) radar [6]. The TM system has been used at MLB ballparks for several years to measure the trajectory and spin vector magnitude for pitches [4]. The Hawk-Eye optical sensor was introduced as MLB's primary pitch-tracking technology in 2020. In addition to the measurements generated by the TM radar, Hawk-Eye provides information about the direction of the spin vector. We show that this additional information can be used to characterize a side force which has been theorized to result from an asymmetric flow separation, aka seam shifted wake, caused by the surface roughness of the ball [2, 16]. The existence of the side force is supported by differences in observed and inferred spin axes [15] as well as by laboratory measurements [14].

2 Baseball Aerodynamics

The trajectory of a baseball traveling through the air depends on the translational velocity vector $\overline{v}$ and the spin vector $\overline{\omega}$ which has a magnitude defined by the spin rate and a direction defined by the spin axis and the right-hand rule as shown in Fig. 1. Gravity pulls

the ball down, drag acts opposite the velocity direction, and the lift and side forces cause the ball to move in directions that are perpendicular to $\overline{v}$. If we define the velocity and spin vector directions by the unit vectors $\widehat{v} = \overline{v}/|\overline{v}|$ and $\widehat{\omega} = \overline{\omega}/|\overline{\omega}|$, then the lift force acts in the direction of $\widehat{\omega} \times \widehat{v}$ and the side force acts in the direction of $\widehat{\omega} - (\widehat{v} \cdot \widehat{\omega})\widehat{v}$. The geometry is shown in Figure 2 where the direction of the undepicted side force is orthogonal to both the drag and lift force directions.

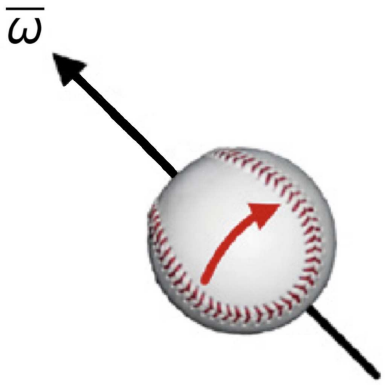

Figure 1: Spin vector $\overline{\omega}$

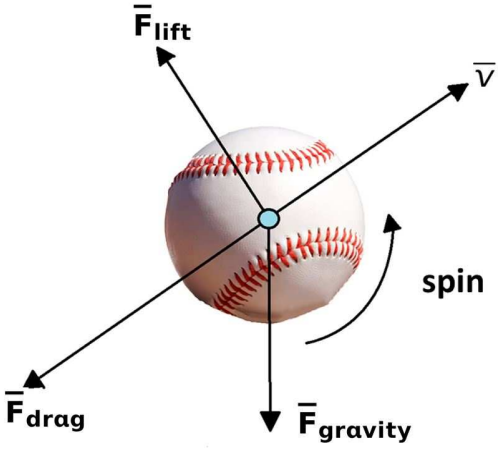

Figure 2: Forces on a spinning baseball in flight

3 The Lift Force

The magnitude of the lift force [12] is given by

$$|\overline{F}_L| = \frac{1}{2}\rho A C_L |\overline{v}|^2 \tag{1}$$

where ρ is the air density, A is the ball cross-sectional area, and C_L is the dimensionless lift coefficient. Increases in C_L increase $|\overline{F}_L|$ and cause larger spin-induced changes in pitch trajectory which typically lead to improved pitch quality [5].

The spin vector $\overline{\omega}$ can be written as

$$\overline{\omega} = \overline{\omega}_{\parallel} + \overline{\omega}_{\perp} \tag{2}$$

where $\overline{\omega}_{\parallel}$ is parallel to $\widehat{v}$ and $\overline{\omega}_{\perp}$ is perpendicular to $\widehat{v}$. $\overline{\omega}_{\parallel}$ is known as the gyro component of the spin and does not contribute to the lift force [13]. The magnitudes of $\overline{\omega}_{\parallel}$ and $\overline{\omega}_{\perp}$ are given by

$$|\overline{\omega}_{\parallel}| = |\overline{\omega}||\widehat{\omega} \cdot \widehat{v}| \tag{3}$$

and

$$|\overline{\omega}_{\perp}| = |\overline{\omega}||\widehat{\omega} \times \widehat{v}|. \tag{4}$$

The spin efficiency [10] measures the proportion of the spin vector magnitude that is transferred to the lift force $\overline{F}_L$. The spin efficiency is defined by

$$E = \frac{|\overline{\omega}_{\perp}|}{|\overline{\omega}|} \tag{5}$$

which simplifies to $E = |\widehat{\omega} \times \widehat{v}|$ using equation (4).

The dimensionless spin parameter S [7] plays an important role in determining C_L and is defined as the ratio of the speed of the ball surface relative to its center to the translational speed of the ball center

$$S = \frac{2\pi R|\overline{\omega}|}{|\overline{v}|} \tag{6}$$

where R is the ball radius.

The lift coefficient C_L can be modeled by

$$C_L = f(S)|\widehat{\omega} \times \widehat{v}| \tag{7}$$

where $f(S)$ is an increasing function of S with $f(0) = 0$ [8]. We have developed a method [6] to generate an estimate of $f(S)$ from TM data. Since the lift and side forces cannot be separated using TM, this estimate will tend to overestimate $f(S)$. This effect, however, is small since the pitches which are most influential in determining the estimate have the largest spin efficiencies and correspondingly small side force contributions. Nevertheless, we address this issue by using large sets of TM data [6] in combination with smaller sets of laboratory optical data [1, 12] to recover the shape of $f(S)$ and use a scale factor that is estimated from Hawk-Eye data to compensate for the effects of the small side force contributions. We showed in [6] that this scale factor is also useful to account for small changes in the baseball from year-to-year. The estimate $\widehat{f}(S, k)$ is represented by a Hill function of the form

$$\widehat{f}(S, k) = \frac{kAS^n}{a^n + S^n} \tag{8}$$

with parameters $A = 0.370$, $n = 1.651$, and $a = 0.137$ where the scale factor k accounts for the aforementioned side force contributions and changes in the baseball.

4 The Side Force

4.1 Sensor Data

The TM sensor coordinate system has its origin at home plate with positive z up, positive y parallel to the ground plane in the direction from the origin to the pitcher's mound, and positive x pointing to the right from the catcher's perspective. The TM system generates a nine-parameter model for each pitch in terms of the three-dimensional acceleration vector $\overline{a} = (a_x, a_y, a_z)$ which is assumed constant over the pitch trajectory and the three-dimensional velocity and position vectors for a point on the trajectory. These parameters

can be used to recover the full path of the pitch from the measured release point using the equations of motion. The system also estimates the magnitude of the spin vector $|\overline{\omega}|$ from the distribution of Doppler shifts. Hawk-Eye generates the same pitch descriptors as the TM system but also provides information about the direction of the spin vector.

4.2 Constraining the Lift Acceleration

As described in Section 2, the acceleration for a pitch is the sum of acceleration components due to gravity, drag, lift, and the side force

$$\overline{a} = \overline{a}_G + \overline{a}_D + \overline{a}_L + \overline{a}_S. \tag{9}$$

Publicly available Hawk-Eye data includes the direction θ_ω of the projection of the spin vector onto the xz-plane. If the unit spin vector is represented by $\widehat{\omega} = (\omega_x, \omega_y, \omega_z)$ then θ_ω is given by

$$\theta_\omega = \text{atan2}(\omega_z, \omega_x). \tag{10}$$

We will show that θ_ω can be used to estimate the three-dimensional spin vector $\overline{\omega}$ and to separate the acceleration components.

The measured θ_ω restricts $\widehat{\omega}$ to a one-parameter family of unit vectors

$$\widehat{\omega}(\omega_y) = (a\cos\theta_\omega, \omega_y, a\sin\theta_\omega) \tag{11}$$

where $a = \sqrt{1-\omega_y^2}$ with $-1 \leq \omega_y \leq 1$. This, in turn, restricts the unit vector in the direction of the lift acceleration to

$$\widehat{a}_L(\omega_y) = \frac{\widehat{\omega}(\omega_y) \times \widehat{v}}{|\widehat{\omega}(\omega_y) \times \widehat{v}|} \tag{12}$$

where $\widehat{v}$ is the unit velocity vector.

The magnitude of the lift acceleration is

$$|\overline{a}_L(\omega_y)| = |(\overline{a} - \overline{a}_G) \cdot \widehat{a}_L(\omega_y)| \tag{13}$$

which enables $C_L(\omega_y)$ to be computed using equation (1) adjusted according to Newton's second law along with fine-grained air density data acquired as described in [6]. Since the velocity vector is not constant, we use the mean velocity over each pitch trajectory for the computation.

4.3 Pitch Groups

We consider the processing of groups of pitches for the 2020 season where each group corresponds to a single pitcher and pitch type such as (Shane Bieber, curveball). The ith group is characterized by $\widehat{v}(i), S(i), C_L(\omega_y, i)$, and $\theta_\omega(i)$ which are the respective means of $\widehat{v}, S, C_L(\omega_y)$, and θ_ω over the pitches in the group where the $\widehat{v}$ mean is renormalized to a unit vector. We also define $\widehat{\omega}(\omega_y, i)$ using (11) with $\theta_\omega = \theta_\omega(i)$.

These descriptors provide two ways to compute the spin efficiency for each group i. Using the definition of equation (5) gives

$$E_1(\omega_y, i) = |\widehat{\omega}(\omega_y, i) \times \widehat{v}(i)| \tag{14}$$

and using equation (7) gives

$$E_2(\omega_y, i, k) = \frac{C_L(\omega_y, i)}{\widehat{f}(S(i), k)} \tag{15}$$

where $\widehat{f}(S, k)$ is given by (8) and k is an unknown scale factor as described in Section 3.

For a given group i and scale factor k, we define $\omega_y^*(i, k)$ as the value of ω_y that minimizes the absolute difference between the two spin efficiency estimates

$$|E_1(\omega_y, i) - E_2(\omega_y, i, k)| \tag{16}$$

and define k^* as the value of k that minimizes

$$\sum_{i=1}^{N} |E_1(\omega_y^*(i, k), i) - E_2(\omega_y^*(i, k), i, k)| \tag{17}$$

where N is the number of pitch groups. A 3-D spin vector direction estimate $\widehat{\omega}^*(i)$ for each group i is then given from equation (11) by setting $\omega_y = \omega_y^*(i, k^*)$ to obtain

$$\widehat{\omega}^*(i) = (a(i)\cos(\theta_\omega(i)), \omega_y^*(i,k^*), a(i)\sin(\theta_\omega(i))) \tag{18}$$

where $a(i) = \sqrt{1-(\omega_y^*(i,k^*))^2}$.

4.4 Separating the Acceleration Components

Let $\overline{a}(i)$ be the mean acceleration vector for pitch group i. The mean drag acceleration for group i can be computed as

$$\overline{a}_D(i) = -\left[(\overline{a}(i) - \overline{a}_G)\cdot\widehat{v}(i)\right]\widehat{v}(i). \tag{19}$$

The lift direction unit vector for the group can be computed by substituting $\widehat{\omega}^*(i)$ into (12) to get

$$\widehat{a}_L(i) = \frac{\widehat{\omega}^*(i)\times\widehat{v}(i)}{|\widehat{\omega}^*(i)\times\widehat{v}(i)|} \tag{20}$$

which gives an estimate of $\overline{a}_L(i)$ as

$$\overline{a}_L(i) = \left[(\overline{a}(i) - \overline{a}_G)\cdot\widehat{a}_L(i)\right]\widehat{a}_L(i) \tag{21}$$

The side acceleration $\overline{a}_S(i)$ can then be estimated using

$$\overline{a}_S(i) = \overline{a}(i) - \overline{a}_G - \overline{a}_D(i) - \overline{a}_L(i) \tag{22}$$

4.5 The Side Force Coefficient

The magnitude of the side acceleration can be written

$$|\overline{a}_S| = \frac{1}{2m}\rho A C_S |\overline{v}|^2 \tag{23}$$

where C_S is the dimensionless side force coefficient [2]. We can estimate $C_S(i)$ for pitch group i by replacing $\overline{a}_S, \rho$, and $\overline{v}$ by their respective means over the pitch group. Figure 3 is a scatterplot of $C_S(i)$ versus $\cos\alpha(i) = |\widehat{\omega}(i)\cdot\widehat{v}(i)|$ for the 334 pitch groups that included at least 200 pitches in 2020 where α is the angle between the spin and velocity vectors.

From equation (3), $\cos\alpha(i)$ is the fraction of the spin vector magnitude that contributes to gyrospin. Sinkers are plotted in red, four-seam fastballs are plotted in green, and other pitch types are plotted in blue. We see that the maximum value of C_S increases approximately linearly with $\cos\alpha$. A side force efficiency ratio could therefore be defined as the fraction of the maximum C_S that a pitch achieves given its $\cos\alpha$. We see that sinkers have the highest value for this ratio. We see that the upper bound for C_S for four-seam fastballs is also approximately linear with a similar slope to the upper bound for sinkers. Approximate upper bound lines for the sinker and four-seam fastball are plotted in Figure 3.

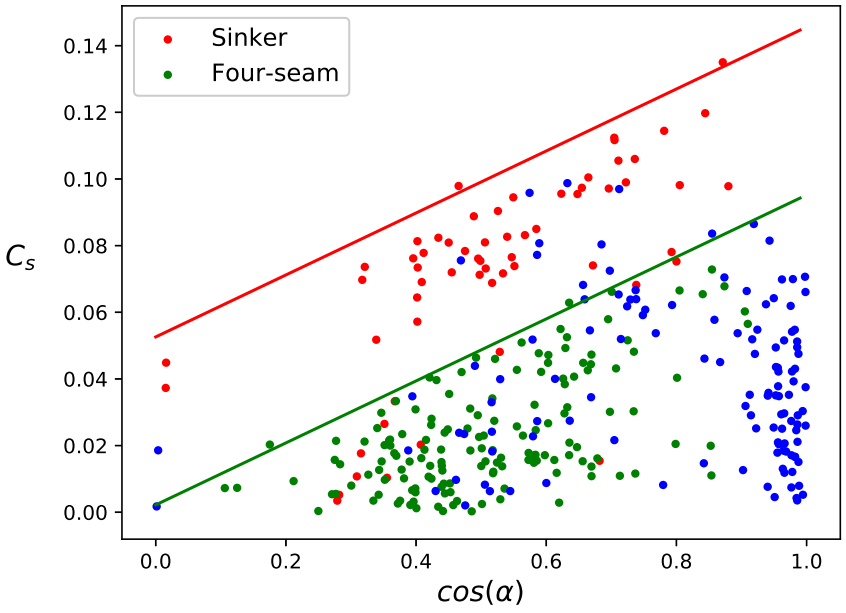

Figure 3: C_S versus $\cos\alpha$ for pitch groups, 2020

4.6 Comparing the Lift and Side Forces

Since the lift and side forces are orthogonal, we can combine equations (1) and (23) to compute the magnitude of their sum as

$$|\overline{F}_L + \overline{F}_S| = R\sqrt{C_L^2 + C_S^2} \tag{24}$$

where

$$R = \frac{\rho A |\overline{v}|^2}{2} \cdot \tag{25}$$

Thus, we can examine the contributions of C_L and C_S to the total force on a pitch. From equation (7) the lift coefficient is given by

$$C_L = f(S) \sin \alpha. \tag{26}$$

Using the process described in Section 4.3 we found $k = 0.962$ for the estimate $\widehat{f}(S, k)$ in equation (8) for the 2020 Hawk-Eye data. We note that this value of k is smaller than the values found in [6] using Trackman data. This is consistent with the ability to remove the side force contributions when computing the lift coefficient model using Hawk-Eye measurements.

The side force coefficient can be expressed as

$$C_S = E_S f_S(\cos \alpha) \tag{27}$$

where E_S is the side force efficiency and $f_S(\cos \alpha)$ is the upper bound to C_S as a function of $\cos \alpha$. We approximate $f_S(\cos \alpha)$ using the equation of the red line in Figure 3 to get

$$f_S(\cos \alpha) = 0.093 \cos \alpha + 0.0526. \tag{28}$$

Figure 4 uses equations (26)-(28) to plot C_L and C_S as a function of α for a typical S value of 0.22 and a side force efficiency E_S of 1.0. We see that C_L increases with α while C_S decreases and that the lift coefficient is larger over most of the range even with the assumption of $E_S = 1$. From equation (3), we see that C_S will decrease as the magnitude of the gyro component of the spin decreases for fixed E_S.

4.7 Movement

Pitch movement [9] [11] is typically defined as the difference between the (x, z) location of a pitch at home plate and the (x, z) location of a pitch thrown at the same speed that is only acted on by gravity. Since the computed movement will depend on the distance the pitch travels, we use the convention of computing movement from $y = 40$ feet. The

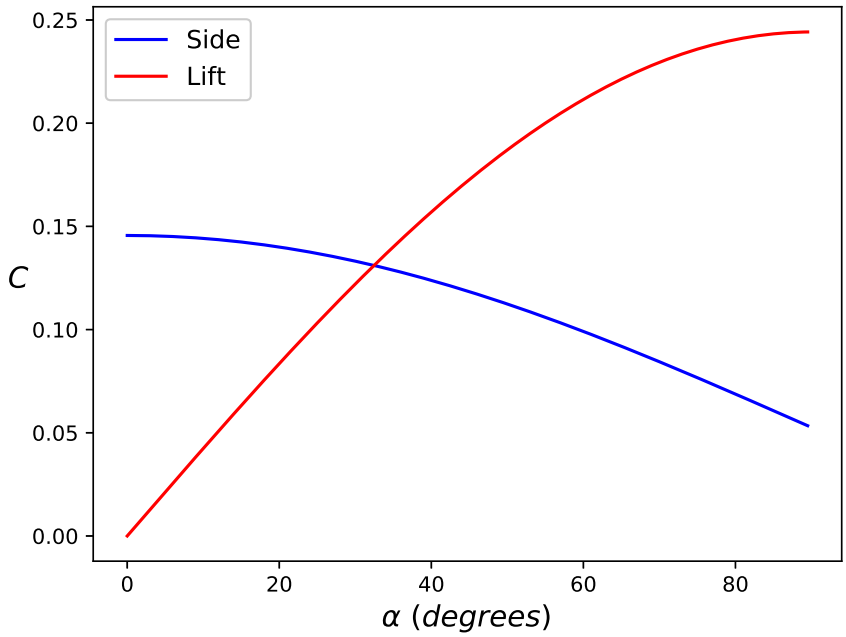

Figure 4: C_L and C_S versus α for $S = 0.22$, $E_S = 1.0$

movement vector for an acceleration vector $\overline{a} = (a_x, a_y, a_z)$ is given by $(\text{pfx\_x}, \text{pfx\_z}) = (0.5a_x t^2, 0.5(a_z - a_g)t^2)$ where t is the time for the pitch to travel from $y = 40$ feet to home plate and a_g is the acceleration due to gravity in the z-direction.

The direction and magnitude of the movement vector have been shown to be key determinants of a pitch's effectiveness [5]. Table 1 displays the average amount of movement due to each force by pitch type. We see that the four-seam fastball has the highest average movement due to the Magnus force while the sinker has the highest average movement due to the side force. The last column in the table provides the average run value of the movement due to the side force per 100 pitches [5]. The side force provides the most value for the split, sinker, and changeup and the least value for the curve.

Figures 5-11 examine the average movement vectors due to the three force components for each pitch type for right-handed and left-handed pitchers. Each plot shows the average movement from the pitcher's point of view with respect to a circle of radius of twelve inches.

Table 1: Average movement in inches due to each force by pitch type

pitch type	Drag	Magnus	Side	Total	SideR/100
Changeup	1.33	7.98	2.40	9.38	0.42
Curve	1.49	8.81	1.28	7.81	0.03
Cutter	1.20	4.28	2.04	5.60	0.26
Four-seam	1.18	9.68	1.16	10.96	0.15
Split	1.42	7.29	2.79	8.66	0.67
Sinker	1.20	9.28	3.42	11.02	0.48
Slider	1.34	3.35	1.52	3.51	0.18

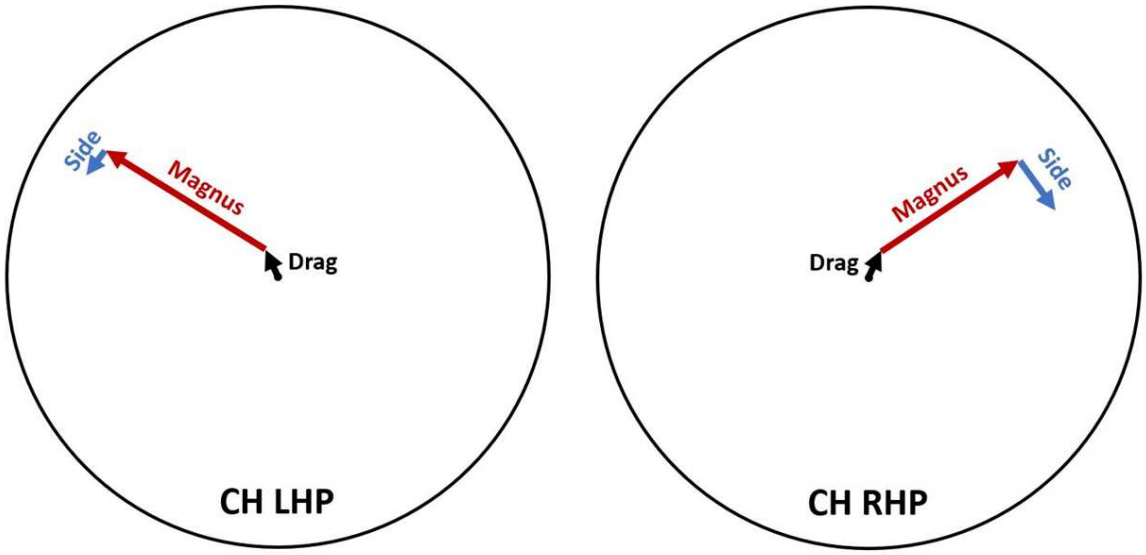

Figure 5: Movement due to Drag, Magnus, and Side forces, Changeup, Pitcher POV

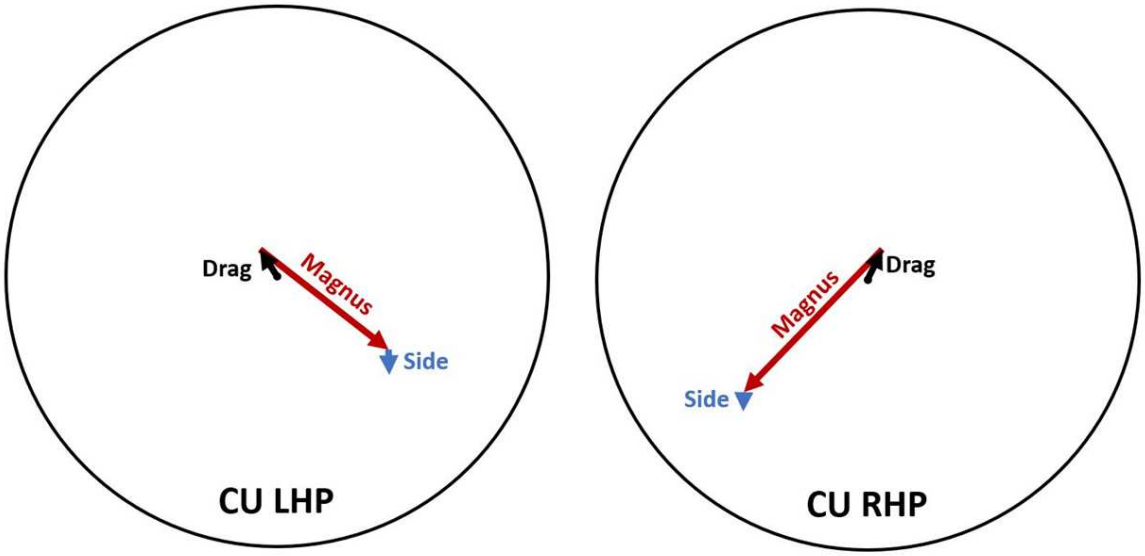

Figure 6: Movement due to Drag, Magnus, and Side forces, Curve, Pitcher POV

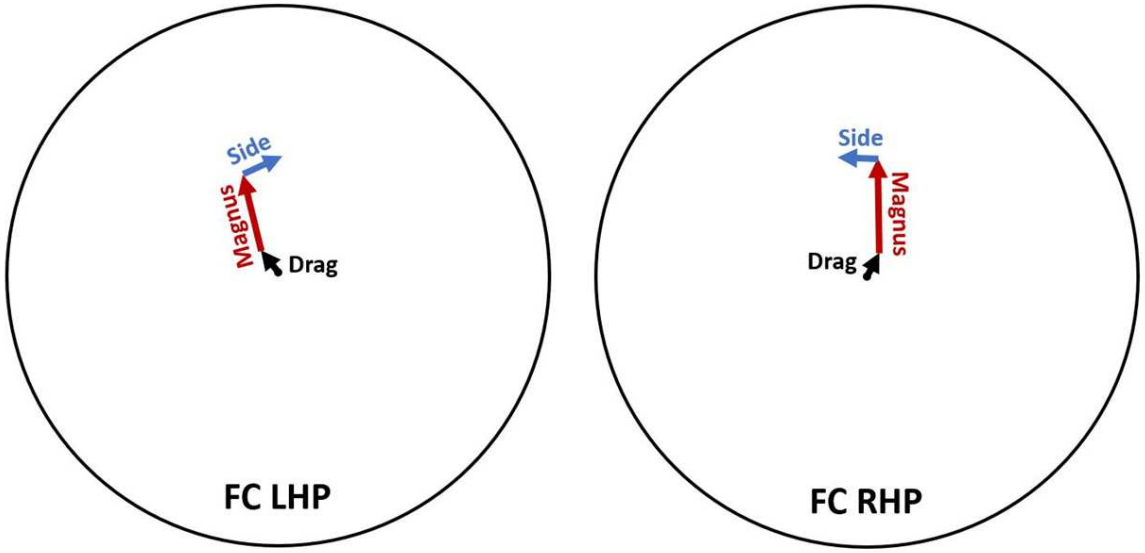

Figure 7: Movement due to Drag, Magnus, and Side forces, Cutter, Pitcher POV

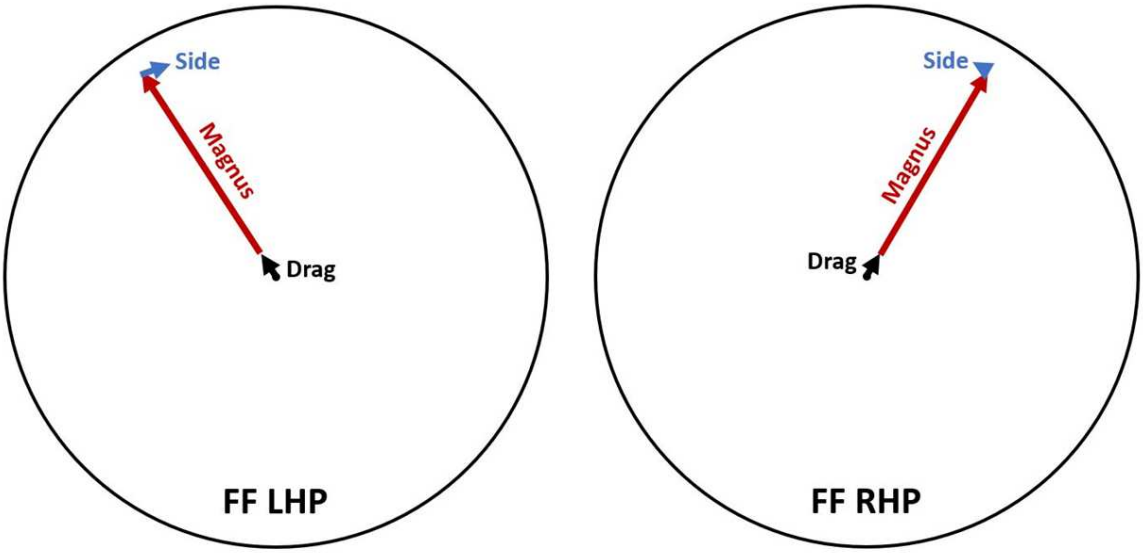

Figure 8: Movement due to Drag, Magnus, and Side forces, Four-seam, Pitcher POV

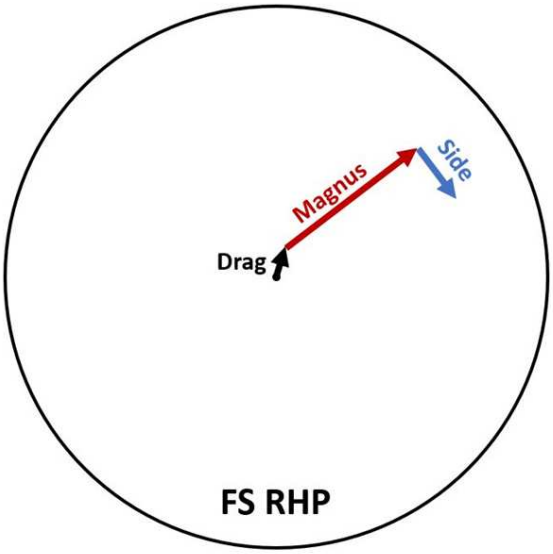

Figure 9: Movement due to Drag, Magnus, and Side forces, Split, Pitcher POV

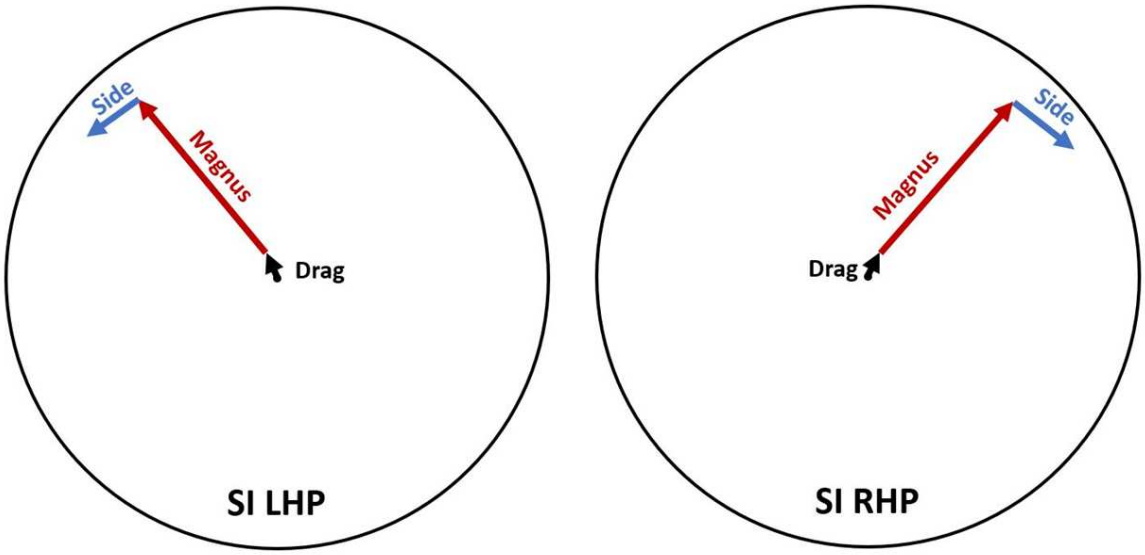

Figure 10: Movement due to Drag, Magnus, and Side forces, Sinker, Pitcher POV

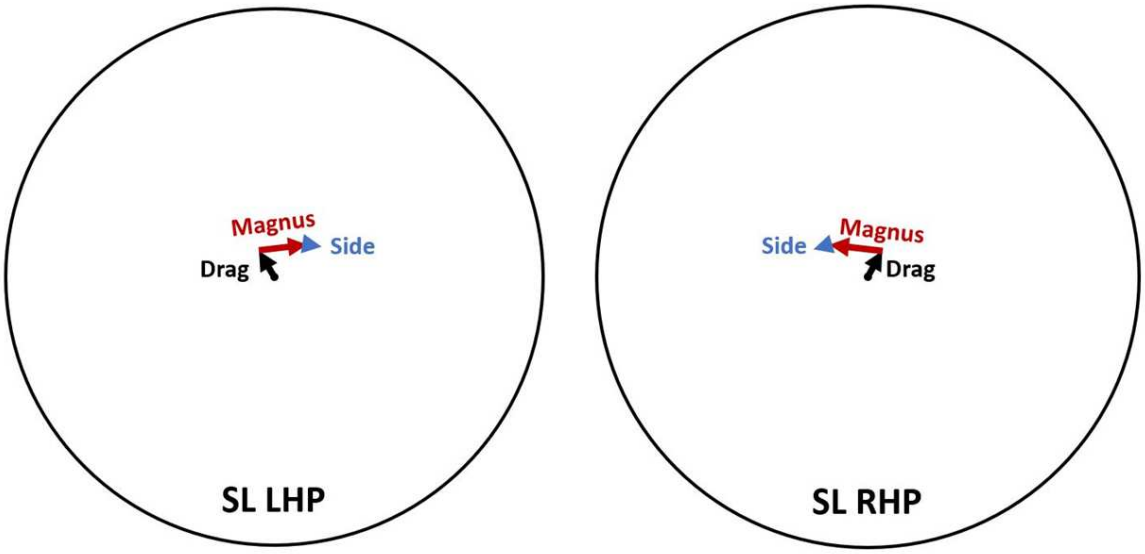

Figure 11: Movement due to Drag, Magnus, and Side forces, Slider, Pitcher POV

Table 2 lists all pitchers who averaged at least 4 inches of side force movement on sinkers in 2020. Tables 3-8 lists all pitchers who averaged at least three inches of side force movement on pitch types other than sinkers. We note that the side force movement of 6.52 inches on the four-seam for Tyler Rogers is uncharacteristic of this pitch type and sources besides MLB including Brooks Baseball classify this pitch as a sinker.

Table 2: Side Force Movement leaders, Sinker, 2020

pitcher	Movement (inches)
Lance Lynn	5.61
Kyle Hendricks	5.46
Adrian Houser	5.32
Lance McCullers	5.25
Jared Hughes	5.09
Dane Dunning	4.97
Gregory Soto	4.75
Zach Britton	4.75
Frankie Montas	4.70
Corbin Burnes	4.69
Alec Mills	4.65
Justus Sheffield	4.61
Spencer Turnbull	4.59
Brad Keller	4.52
Aaron Civale	4.49
Brandon Kintzler	4.48
Ryan Weber	4.32
Brandon Woodruff	4.26
Patrick Corbin	4.00

Table 3: Side Force Movement leaders, Changeup, 2020

pitcher	Movement (inches)
Pablo Lopez	4.67
Phillips Valdez	4.67
Kyle Gibson	3.83
Zac Gallen	3.70
Luis Castillo	3.64
Dylan Bundy	3.52
Luke Weaver	3.46
Dallas Keuchel	3.21
Logan Webb	3.03
Carlos Carrasco	3.02
Johnny Cueto	3.01

Table 4: Side Force Movement leaders, Curve, 2020

pitcher	Movement (inches)
Framber Valdez	4.51
Jose Berrios	3.17

Table 5: Side Force Movement leaders, Cutter, 2020

pitcher	Movement (inches)
Jon Lester	3.87
Wander Suero	3.38
Yusei Kikuchi	3.37
Ryan Yarbrough	3.32
Trevor Bauer	3.31
Will Harris	3.17

Table 6: Side Force Movement leaders, Four-seam, 2020

pitcher	Movement (inches)
Tyler Rogers	6.52
Mike Minor	3.50
Alex Cobb	3.33
J.B. Wendelken	3.25
Anthony Kay	3.19
Brent Suter	3.17
Brad Keller	3.00

Table 7: Side Force Movement leaders, Split, 2020

pitcher	Movement (inches)
Alex Cobb	3.08

Table 8: Side Force Movement leaders, Slider, 2020

pitcher	Movement (inches)
Matt Wisler	4.10
Mike Clevinger	3.96

References

[1] L. Alaways and M. Hubbard. Experimental determination of baseball spin and lift. *Journal of Sports Sciences*, 19:349–358, 2001.

[2] R. Cross. Aerodynamics in the classroom and at the ball park. *Am. J. Phys.*, 80(4):289–297, 2012.

[3] R. Gray. Behavior of college baseball players in a virtual batting task. *Journal of Experimental Psychology: Human perception and performance*, 28(5):1131–1148, 2002.

[4] G. Healey. The new Moneyball: How ballpark sensors are changing baseball. *Proceedings of the IEEE*, 105(11):1999–2002, 2017.

[5] G. Healey. A Bayesian method for computing intrinsic pitch values using kernel density and nonparametric regression estimates. *Journal of Quantitative Analysis in Sports*, 15(1):59–74, March 2019.

[6] G. Healey and L. Wang. (Aug. 18, 2020). Combining radar, weather, and optical measurements to model the dependence of baseball lift on spin and surface roughness [Online]. Available: vixra.org/pdf/2008.0131v1.pdf.

[7] R. Mehta and J. Pallis. Sports ball aerodynamics: effects of velocity, spin, and surface roughness. In F. Froes and S. Haake, editors, *Materials and Science in Sports*, pages 185–197. TMS, 2001.

[8] T. Nagami, T. Higuchi, H. Nakata, T. Yanai, and K. Kanosue. Relation between lift force and ball spin for different baseball pitches. *Journal of Applied Biomechanics*, 32:196–204, 2016.

[9] A. Nathan. (August 27, 2018). Pitch movement, spin efficiency, and all that [Online]. Available: tht.fangraphs.com/pitch-movement-spin-efficiency-and-all-that.

[10] A. Nathan. (March 31, 2015). All spin is not alike [Online]. Available: www.baseballprospectus.com/article.php?articleid=25915.

[11] A. Nathan. (Oct. 21, 2012). Determining pitch movement from PITCHf/x data [Online]. Available: baseball.physics.illinois.edu/Movement.pdf.

[12] A. Nathan. The effect of spin on the flight of a baseball. *Am. J. Phys.*, 76(2):119–124, 2008.

[13] A. Nathan and D. Baldwin. An analysis of the gyroball. *Baseball research journal*, 36:77–80, 2007.

[14] A. Smith and B. Smith. Using baseball seams to alter a pitch direction: the seam shifted wake. *Proceeedings of the Institution of Mechanical Engineers Part P: Journal of Sports Engineering and Technology*, October 2020.

[15] B. Smith, A. Nathan, and H. Pavlidis. (Nov. 5, 2020). Not just about Magnus anymore [Online]. Available: baseballprospectus.com/news/article/62912/not-just-about-magnus-anymore.

[16] R. Watts and A.T. Bahill. *Keep your eye on the ball.* W.H. Freeman and Company, 1990.